

Megacrystic zircon with planar fractures in miaskite-type nepheline pegmatites formed at high pressures in the lower crust (Ivrea Zone, southern Alps, Switzerland)

URS SCHALTEGGER^{1,*}, ALEXEY ULIANOV², OTHMAR MÜNTENER², MARIA OVTCHAROVA¹,
IRENA PEYTCHEVA^{1,3}, PIERRE VONLANTHEN², TORSTEN VENNEMANN², MARCO ANTOGNINI⁴
AND FABIO GIRLANDA⁴

¹Section of Earth and Environmental Sciences, University of Geneva, 13 rue des Maraichers, 1205 Geneva, Switzerland

²Institute of Earth Sciences, University of Lausanne, Geopolis, 1015 Lausanne, Switzerland

³Geological Institute, Bulgarian Academy of Science, Acad. G. Bonchev str., bl.24, 1113 Sofia, Bulgaria

⁴Museo Cantonale di Storia Naturale, Viale Cattaneo 4, 6900 Lugano, Switzerland

ABSTRACT

Trace element, Hf, and O isotopic composition and U-Pb geochronological data are reported for zircon megacrysts found in miaskitic (zircon, biotite, plagioclase-bearing) nepheline syenite pegmatites from the Finero complex in the Northeastern part of the Ivrea-Verbano Zone, southern Alps. Zircon from these pegmatites was reported to reach up to 9 cm in length and is characterized by ~100 µm spaced planar fractures in different directions. Small volumes of these highly evolved alkaline melts intruded into the lower crust and were emplaced within amphibole peridotites and gabbros between 212.5 and 190 Ma. A zircon crystal of 1.5 cm size records a systematic core-to-rim younging of 4.5 Ma found by high-precision CA-ID-TIMS ²⁰⁶Pb/²³⁸U dating of fragments, and of 8.7 Ma detected by laser ablation ICP-MS spot dating. Volume diffusion at high temperatures was found to be insufficient to explain the observed within-grain scatter in dates, despite the fact that the planar fractures would act as fast diffusion pathways and thus reduce effective diffusion radii to 50 µm. The U-Pb system of zircon is therefore interpreted to reflect an episodic protracted growth history.

These high-pressure miaskites probably formed by episodic, low-degree decompression melting of a metasomatically enriched mantle source and subsequent crystallization in the lower crust at volatile saturation with explosive volatile release, evidenced by their brecciated texture in the field and by the occurrence of planar fractures in zircon. They point to the existence of a long-lived period of heat advection in the deep crust by highly differentiated melts from enriched, lithospheric mantle.

Keywords: Miaskitic pegmatite, zircon megacrysts, U-Pb, planar fractures, southern Alps, diffusion modeling, volatile explosions

INTRODUCTION

The mineral zircon (ZrSiO₄) can form exceptionally large crystals in various different rocks: zircon crystals of up to 25 cm size have been reported from carbonatites (Black and Gulson 1978; Crohn and Moore 1984); centimeter-sized megacrysts are known from granitic pegmatites (Lacroix 1922; Besairie 1966), alkaline basalts (Hollis and Sutherland 1985; Yu et al. 2010), and from kimberlites (e.g., Schärer et al. 1997; Page et al. 2007, and references therein). Kimberlite zircons are at least partly interpreted as fragments of coarse-grained, LILE, and HFSE enriched mantle veins formed by crystallization of melts of lamproite or kimberlite affinity at mantle depths (so-called MARID's; Dawson and Smith 1977; Bayly et al. 1979; Waters 1987; Konzett et al. 1998) entrained by the rising kimberlite magma. However, most studies about megacrystic zircon focused on nepheline syenites and their associated pegmatites and pneumatolytic-hydrothermal veins, such as at Seiland (Pedersen et al. 1989; Weiss 2011), Khibiny and Lovozero (e.g., Arzamast-

sev et al. 2008), and in the Ilmeny and Vishnevye Mountains, which is the type locality for miaskite (Popov and Popova 2006, and references therein). Other prominent examples, especially from tectonized nepheline syenites, were summarized by Ashwal et al. (2007). Nepheline-syenite pegmatites are usually part of alkaline magmatism associated with intracontinental rifts, such as the Oslo Rift (e.g., Andersen et al. 2010) and the Gardar rifting province of Greenland (Upton and Emeleus 1987). Zircon is a characteristic mineral in miaskitic rocks. Along the miaskitic-agpaitic differentiation trend of nepheline-bearing syenitic magmas, zircon gets replaced by Zr-bearing silicates at higher activities of sodium, water, and halogens forming minerals such as eudialyte, rosenbuschite, or catapleite (Andersen et al. 2010). The described mineral parageneses in the literature are known to have crystallized at moderate or low pressures (e.g., 0.1 GPa for the Larvik and Ilímaussaq complexes, Andersen et al. 2010; Konnerup-Madsen and Rose-Hansen 1984; Markl et al. 2001), with some localities still preserving remnants of the volcanic suite pre-dating the intrusion of nepheline syenite (e.g., Arzamastsev et al. 2008).

In this study, zircon crystals from a spectacular occurrence

* E-mail: urs.schaltegger@unige.ch

of megacrystic miaskite-type (zircon, biotite, and nepheline-bearing) alkaline pegmatites from the northeastern termination of the South-Alpine, high-grade Ivrea-Verbano Zone (IVZ; Fig. 1) are examined. These pegmatites seem to have formed through differentiation of partial melts of a metasomatized lithospheric mantle during Triassic lithospheric thinning. Zircon crystals up to 9 cm in length were previously reported (Girlanda et al. 2007; Weiss et al. 2007). We present data from several up to centimeter-sized, short prismatic zircon crystals, collected from small pods of these alkaline pegmatites that intruded between 212.5 and 190 Ma in the mafic-ultramafic Finero Complex, a 15 km long inlier in the IVZ lower crust.

Some of the studied crystals present striking features, such as (1) U-Pb age differences up to 8.7 Ma from laser ablation ICP-MS spot dating on a single crystal, and up to 4.5 Ma from CA-ID-TIMS analyses on crystal fragments; and (2) conspicuous planar fractures running through the crystals along different directions. We will discuss two hypotheses, namely whether (1) such large intracrystal age differences are resulting from pulsed growth with long intermediate periods of stagnation due to repetitive injection of zircon-saturated melt or fluid, or, (2) whether age differences may be explained by diffusion processes removing radiogenic lead at high temperatures and pressures over long periods of time. The studied zircon bearing pegmatites are to the best of our knowledge the first report on high-pressure crystallization of a zircon-bearing miaskitic, alkaline pegmatite, while known occurrences linked to nepheline-syenite intrusions were forming at shallower crustal levels. We have to assume elevated ambient temperatures and pressures in both mantle and lower crustal units of the Finero area in between 212 and 190 Ma; sapphirine-spinel

equilibrium temperatures of 980–1030 °C were reported from leucogabbroic veins cutting phlogopite-bearing peridotite (Sills et al. 1983; Giovanardi et al. 2013; Zanetti, oral comm.). The further thermal evolution of this area is approximated by a U-Pb age of 181 ± 4 Ma from rutile of the IVZ (Zack et al. 2011), dating the cooling to around 600–700 °C (Cherniak et al. 2007).

Crystallization of the studied zircons at high pressures is also indicated by the conspicuous presence of planar fractures, which are otherwise typically known from kimberlitic and impactite-hosted zircons. We suggest that the planar fractures may result from sudden volatile release in the host pegmatite and discuss whether they may have acted as diffusion pathways along which radiogenic lead was removed.

THE TRIASSIC AGE OF THE FINERO MAFIC-ULTRAMAFIC COMPLEX

The studied zircon crystals originate from alkaline pegmatites within hornblende peridotites and gabbros at the eastern termination of the Finero ultramafic-mafic complex (Centovalli area, southern Switzerland/northern Italy; Fig. 1). This complex is included in the high-grade, South-Alpine polymetamorphic basement of the IVZ, interpreted to represent a ~30 km thick section of the Mesozoic passive margin of the Adriatic plate (Rutter et al. 2007). The IVZ hosts several ultramafic-mafic bodies, the Finero body being the easternmost and largest one. The Finero Complex has been described as a large antiform with a distinct uppermost-mantle to lower-crustal “stratigraphy” (see descriptions in Siena and Coltorti 1989, Giovanardi et al. 2013, and Zanetti et al. 2013): The center of the antiform hosts a mantle-derived phlogopite peridotite, surrounded by a lower

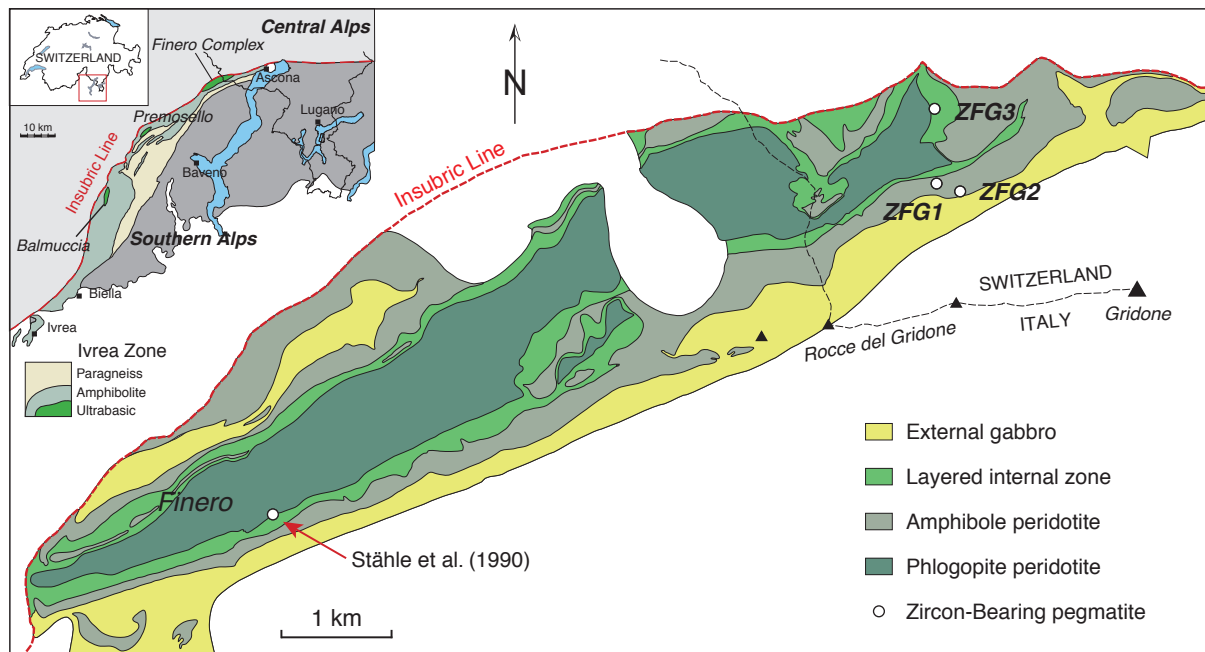
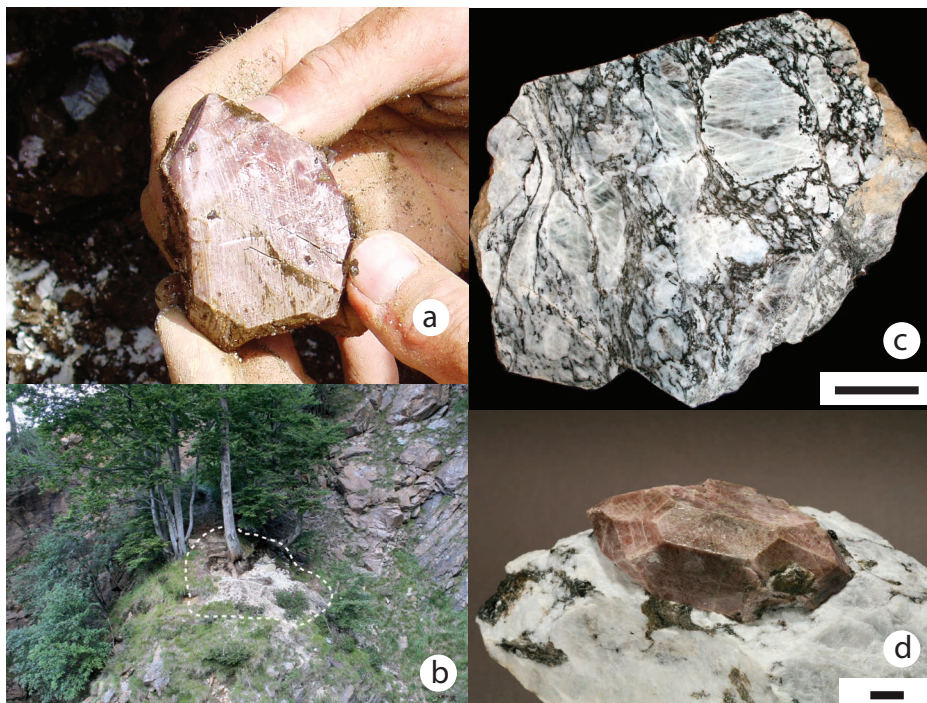


FIGURE 1. Geological sketch map of the Finero complex with main lithologies; sample localities are indicated (ZFG1 to ZFG3) as well as the syenite pegmatite locality from Stähle et al. (1990). Inset: Geological map showing the position of the Finero complex adjacent to the Insubric Line, which is the main suture between central Alps (European plate) and southern Alps (Adriatic plate). Both modified from Girlanda et al. (2007).

► **FIGURE 2.** (a) A 4 cm long zircon from pegmatite ZFG1 showing conspicuous planar fracturing parallel to *c* axis; (b) outcrop photograph showing the original extension of the pegmatite body delivering the ZFG2a, b, and c crystals, prior to excavations for scientific purposes by the Museum of Natural History of Lugano; (c) polished rock slab displaying the fracturing of Na-rich first magmatic phase with nepheline and albite crystals by K-rich melt crystallizing biotite, showing ductile deformation in the left part. Scale bar = 10 cm; (d) an example of a large zircon from pegmatite ZFG2b; Scale bar = 1 cm.



crustal Mafic Complex. The latter is differentiated into (1) a Layered Internal Zone, featuring amphibolites, garnet-bearing gabbros, anorthosites, pyroxenites, and rare peridotites; (2) lower crustal cumulus peridotites (“Amphibole peridotite” in Fig. 1), which are markedly different from the mantle-derived phlogopite peridotites in the center, but hosting sometimes similar looking harzburgites; and (3) External Gabbros (mainly consisting of amphibole gabbro and diorite) that intruded into the lower crustal units.

Recent geochronological work (Zanetti et al. 2013) evidenced that the emplacement of the External Gabbros of the Finero Mafic Complex occurred at 232 ± 3 Ma, which corroborates numerous earlier dating attempts that revealed Triassic ages, for both mantle and intrusive rocks of the Finero complex (e.g., Grieco et al. 2001; Lu et al. 1997). The more westerly ultramafic bodies of the Ivrea Zone (Balmuccia, Premosello; inset Fig. 1), in contrast, are considered to be presumably emplaced at lower crustal levels during the 340–300 Ma Variscan orogeny before the lower Permian intrusion of the Mafic Complex (Peressini et al. 2007), despite some radio-isotopic data pointing to possibly younger ages at around 250–260 Ma (e.g., Gebauer et al. 1992; Mayer et al. 2000).

The Finero mantle unit, i.e., the phlogopite peridotite, was overprinted by several metasomatic events (see Zanetti et al. 2013; Giovanardi et al. 2013; and references therein), leading to the formation of phlogopite in the peridotites that were dated at 220 to 190 Ma (Hartmann and Wedepohl 1993; Hunziker 1974), and of chromitite veins featuring anhedral zircon dated at 204 to 208 Ma (von Quadt et al. 1993; Grieco et al. 2001). Alkaline pegmatites and plagioclase-rich dikes and bodies of Triassic age were previously reported (Stähle et al. 1990; 225 ± 13 Ma; Grieco et al. 2001; 195–202 Ma).

DESCRIPTION OF THE PEGMATITES AND THEIR ZIRCONS

We report chemical and isotopic data of zircon from three pegmatite occurrences: ZFG1 and ZFG2 occur within the amphibole peridotites of the Inner Layered Series, close to the contact with cumulus harzburgites, while ZFG3 is hosted within gabbros of the Layered Internal Zone (Fig. 1).

Pegmatite ZFG1 is hosted by a serpentinized and weathered peridotite; it contains albite, biotite, and highly fractured and shattered zircon, occurring in 5–9 cm large masses containing centimeter-large, transparent, and inclusion-free fragments (Weiss et al. 2007). The zircons show equally spaced planar fractures in different directions [Fig. 2a; orientations parallel to (100), (010), and (211)]. Since no euhedral crystals could be sampled, five gem-quality fragments were randomly selected from a gem-quality domain of a shattered big zircon crystal and analyzed for U and Pb isotopes. The other studied pegmatites contain both nepheline and albite, whereas ZFG1 is albite-bearing only.

Pegmatite ZFG2 is situated within strongly weathered peridotite and contains an exceptional mineral assemblage with abundant zircon crystals, some up to 9 cm in length, beside nepheline, albite, biotite, zircon, apatite, sodalite, magnetite, hercynite, ferrocolumbite, and corundum (Weiss et al. 2007). The pegmatite lens had an original volume of some 50 to 100 m³ (Fig. 2b). The pegmatite displays a macroscopic texture that indicates a formation during two phases: In first instance, a miaskite-type melt first crystallized subhedral megacrysts and lense-shape nepheline crystals up to 50 cm in size, together with albite megacrysts of up to 30 cm. in a second stage, more potassic (and probably volatile-saturated) melt was fracturing the pre-existing nepheline and albite crystals, and was filling the interstitial space and fractures by a much finer grained matrix

mainly consisting of biotite±albite. The second stage seems to be related to ductile deformation (Fig. 2c). The breccia-like structure may be compared to hydrofracturing in magmatic systems and will be used as an argument for involving sudden volatile release at mantle or lower crustal depth.

Zircon crystallized in large grains of brown to pink color during both phases (Fig. 2d). The morphology suggests higher zircon crystallization temperatures for the Na-dominated phase; the presence of {211} bi-pyramids of zircon enclosed in biotite may indicate lower temperatures during the K-dominated fracturing phase (Girlanda et al. 2007).

Zircons of ZFG2 were randomly selected from a collection of isolated crystals, representing grains without recognizable intergrowth with matrix minerals. They are pink to brownish in color, non-transparent, and show a comparable degree of planar fracturing. Three crystals have been studied from this sample, termed ZFG2a, ZFG2b, and ZFG2c. Each is measuring some 1 to 1.5 cm in length, is of pink to brownish color and fragmented into lozenges by a multitude of planar fractures (PFs; Fig. 3). The PFs in crystal ZFG2b exhibit clearly one distinct direction {211}, in addition of a multitude of other less-developed directions. Grain ZFG2a was crushed in a small agate mortar and fragments were randomly selected for CA-ID-TIMS U-Pb dating, whereas grains ZFG2b and ZFG2c were embedded into epoxy resin, cut down to an approximately equatorial section and polished for further in situ imaging and microanalysis (see Fig. 3).

Pegmatite ZFG3 is contained by a gabbroic host rock, is less megacrystic compared to the two other samples and contains nepheline, albite, apatite, and corundum. The maximum 5 cm large albite and nepheline crystals are separated by a network of chlorite; the same mineral constitutes dark interstitial patches between the other minerals. This sample being closest to the Insubric Line, we assume that the chlorite formed as an alteration product of biotite during Alpine metamorphism. Sample ZFG3 was manually crushed and zircon crystals separated by methylene iodide and were selected for further analysis using a binocular microscope. Twelve zircons from two subpopulations of pink and colorless transparent zircons, respectively, were analyzed for U-Pb age determinations, 6 pink single crystals of

100–200 µm length, and 6 colorless fragments of initially larger zircon crystals.

RESULTS

Analytical techniques are described in detail in the electronic supplementary material¹, which is available on deposit.

Cathodoluminescence and backscattered electron imaging of analyzed zircon

Representative grains or fragments of zircon from all three samples were imaged by panchromatic cathodoluminescence (CL) before any further thermal treatment, to characterize the internal textures. The zircon fragments of sample ZFG1 did not reveal any texture in CL. The two 1.5 cm long crystals ZFG2b and ZFG2c are dissected by several orientations of parallel fractures, already visible macroscopically (Fig. 3). The CL images (Figs. 4a–4d) show a mosaic-like texture formed by 100–200 µm large homogenous domains with slightly different CL intensity, limited by open fractures and indicating late (Alpine?) brittle fracturing of the grains. In several cases, semi-quantitative EDS analyses were carried out on the material filling these fractures, which turned out to be either albite (Fig. 4e; BSE image) or high-Th, U zircon (Fig. 4f; BSE image), pointing to the fact that these fractures may initially have been formed at elevated temperatures from late- to post-magmatic melt or fluid. Post-magmatic pneumatolytic and hydrothermal processes forming mineralized veins (including zircon) have frequently been reported from alkaline complexes and nepheline syenite massifs (e.g., Arzamastsev et al. 2008). The CL image of ZFG2b (Fig. 4a) shows irregular patchy distribution without a relation to fractures, with high-CL patches of 50–100 µm size. Only the outermost 200 µm display fine oscillatory zoning without a sharp boundary toward the more internal, homogeneous domain (Fig. 4d).

Two CL images of zircons from ZFG3 are shown in Figures 4g and 4h. They display simple sector zoning without any trace of neither oscillatory growth zones, nor any of the above features such as planar fractures. Such sector or broad band planar zoning is typical for growth at elevated pressures in oceanic and continental arc gabbros, kimberlites, or granulite-facies lower crustal rocks (e.g., Schaltegger et al. 1999; Corfu et al. 2003; Grimes et al. 2009).

Electron backscatter diffraction

To test whether the mosaic-like texture shows a coherent structural orientation, an EBSD cumulative misorientation map was acquired from crystal ZFG2c (Fig. 5). The EBSD map indicates no important misfit beyond 2–3°; the apparent misfit in marginal portions may be considered as an artifact of structural damage during the preparation of the sample at the polishing stage. ZFG2c does therefore not display a typical mosaic texture and is considered to be a near-perfect mono-crystal without evidence for different lattice orientations.

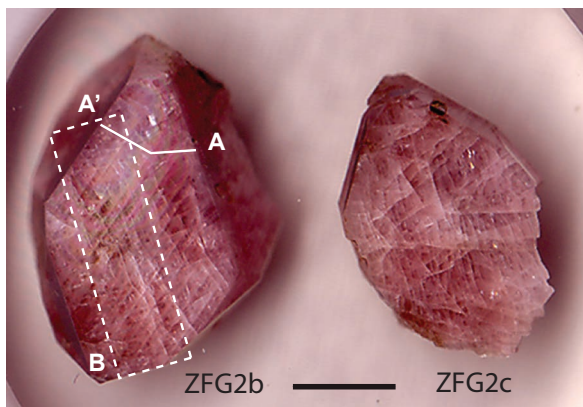


FIGURE 3. Optical picture of zircons ZFG2b and ZFG2c embedded in epoxy resin before analysis. A-A' trace of laser ablation ICP-MS trace element profile in Figure 6; B = trace of the U-Pb ID-TIMS transect drawn in Figure 7c. Scale bar = 1 cm.

¹ Deposit item AM-15-103, Analytical techniques, including supplemental figure and tables. Deposit items are stored on the MSA web site and available via the American Mineralogist Table of Contents. Find the article in the table of contents at GSW (ammin.geoscienceworld.org) or MSA (www.minsocam.org), and then click on the deposit link.

Trace element composition of zircon

The results of trace-element analysis of crystals ZFG2b and ZFG2c are summarized in Supplemental Table 1¹ and Figure 6. A trace element profile has been analyzed across crystal ZFG2b (line A-A' on Fig. 6a) across a domain boundary with slightly different CL intensity. The results for Yb, U, Th, and Nb are displayed in Figure 6b. The low-CL margins show a two- to threefold enrichment in the heavy elements U, Th, and of 50% in Yb relative to the central portion with slightly higher luminescence, whereas Nb does not exhibit any significant variation across the profile. The Nb/Ta ratio, however, changes from about 60 in the central part to about 35 in the margin (Supplemental Table 1¹). This variation is entirely caused by variable Ta contents. The outermost rim is again low in Yb, U, and Th, and may correspond to the oscillatory-zoned rim in Figure 4d. REE analyses of this transect through zircon ZFG2b are shown separately for inner bright-CL, marginal low-CL and outermost rim spot locations (Fig. 6c). The different zones have slightly

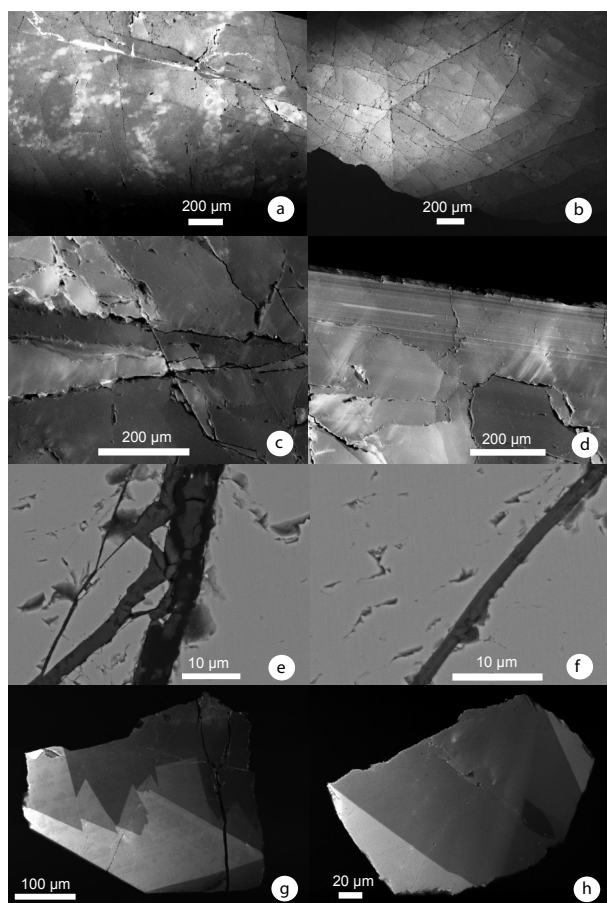


FIGURE 4. CL and BSE images. (a) Patchy CL emission in ZFG2b; (b) mosaic structure in CL (ZFG2c); (c) mosaic structure limited by open fractures (CL, ZFG2b); (d) fine oscillatory CL zoning in the outermost 200 μm of ZFG2b; (e) fracture filled with albite (BSE; ZFG2b); (f) fracture filled with high-Th, U zircon (BSE, ZFG2b); (g) CL image of a 50 μm large pink zircon from ZFG3; (h) CL image of a 150 μm large transparent zircon fragment of ZFG3, both showing undisturbed sector zoning.

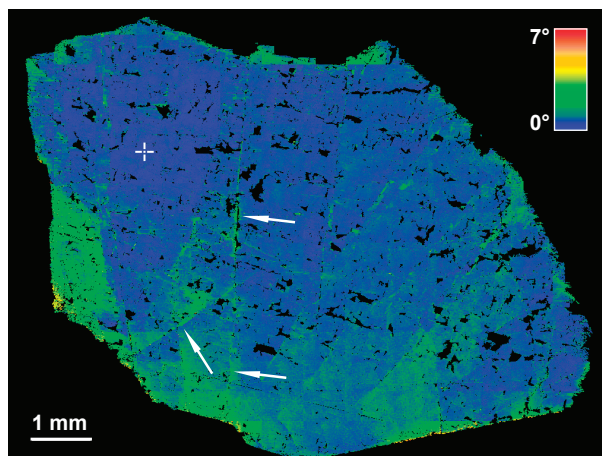
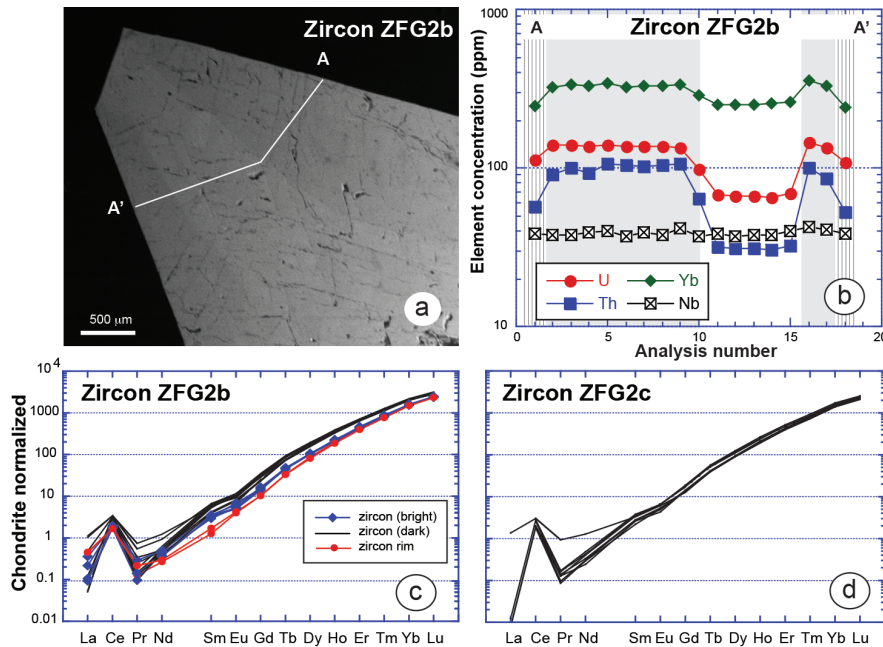


FIGURE 5. EBSD cumulative misorientation map of sample ZFG2c showing the relative change in crystallographic orientation from a user-defined reference point (white cross, blue) to a maximum of 7° (red). The map shows that the whole grain lattice lies within a 3° misorientation interval (blue to green) with maxima located along crystal fractures (arrows). The map was intentionally scaled over 7° (instead of 3°) to reduce the image noise resulting from tiny differences in orientation measurements between contiguous pixels and to limit treatment-related defects, such as scratches. The misorientation of ~2° (green) that can be observed in the borders of the grain (in contact with the weak and non-conducting epoxy resin) are either due to charging effects, or to a slight shift of the EBSD pattern center caused by the preferential polishing of crystal edges.

variable REE concentrations with a weak negative Eu anomaly ranging from 0.47–0.75 (Supplemental Table 1¹), a common positive Ce anomaly, but slightly variable La, Pr, Nd, and Sm, probably caused by microinclusions of albite. Trace and rare earth element analyses on crystal ZFG2c yielded a very similar result (Fig. 6d). The REE patterns are representative of zircon from a granitic melt, the Zr/Hf ratios of ~53 are, however, higher than any chondritic, crustal or basaltic value (Schärer et al. 1997; Wang et al. 2010), but typical for alkaline liquids and their zircons (Linnen and Keppler 2002).

U-Pb spot dating of zircon by laser ablation ICP-MS

To assess the duration of growth of 1.5 cm large zircon crystals we have performed laser ablation-ICP-MS U-Pb dating on crystal ZFG2b (Supplemental Table 2¹; Fig. 7a). A 3020 μm long profile following the A-A' trace in Figure 6a was analyzed with a total of 72 laser spots, split in two halves: a 2330 μm long first part had to be interrupted due to the presence of a 500 μm wide zone of cracks and was completed by another 130 μm long transect toward the core. The $^{206}\text{Pb}/^{238}\text{U}$ dates reveal a resolvable difference between 197 Ma (± 2.5 Ma typical 2σ) for 2 points in the outermost, oscillatory-zoned rim, and up to 205.7 Ma, i.e., over 8.7 Ma. Excluding the two younger outermost rim points and two outliers (all marked in black in Fig. 7a), a mean $^{206}\text{Pb}/^{238}\text{U}$ age of 202.54 ± 0.46 Ma (95% c.l.; MSWD = 2.2) is calculated. The slightly elevated MSWD is in agreement with the analytical scatter of the 91500 standard (MSWD = 2.0; Supplemental Fig. 1¹), indicating the presence of some additional, unresolved



◀ **FIGURE 6.** Results of laser ablation ICP-MS trace and rare earth element analyses: (a) CL image of the tip of crystal ZFG2b with indication of the trace element transect A-A'; (b) variation of U, Th, Yb, and Nb along transect A-A'; gray bands correspond to the low-CL zones of Figure 6a, hatched bands represent the outermost, oscillatory rim visible in Figure 4d; (c) REE patterns of zircon ZFG2b for central, marginal, and outermost rim spot locations; (d) REE patterns of zircon ZFG2c for comparison.

source of error in our data set. The data therefore reflect analytical scatter only and do not resolve any significant age difference within the central portion of the grain. The zircons therefore do not support the hypothesis of episodic or continuous growth from core to rim over millions of years, except for the presence of a thin young overgrowth rim at around 197 Ma.

High-precision U-Pb dating of zircon using CA-ID-TIMS techniques

High-precision U-Pb data were obtained using air-abrasion for sample ZFG1, and chemical abrasion, isotope dilution thermal ionization mass spectrometry (CA-ID-TIMS) techniques for zircons of samples ZFG2 and ZFG3 (for results see Supplemental Table 3¹).

ZFG1. Five air-abraded fragments of a strongly shattered but clear, gem-quality zircon containing 19 to 38 ppm of U and a Th/U ratio of 0.5 were analyzed for U and Pb isotopes using analytical protocols valid in 1999 (see description in electronic appendix¹). The five analyses resulted in a mean $^{206}\text{Pb}/^{238}\text{U}$ age of 212.46 ± 0.33 Ma (95% c.l.; MSWD = 0.66; Fig. 7b).

ZFG2a. A randomly picked crystal from the zircon-megacrystic pegmatite was crushed, and 5 chemically abraded and randomly chosen fragments analyzed for their U-Pb age. The $^{206}\text{Pb}/^{238}\text{U}$ data scatter between 207.6 ± 0.21 and 209.5 ± 0.15 Ma (2σ ; Fig. 7c), at low U concentrations of 23 to 67 ppm and Th/U ratios of 0.6 to 0.8.

ZFG2b. The recognized differences in the U-Pb dates from LA-ICP-MS spot dating (Fig. 7a) as well as from ID-TIMS dating of ZFG2a (Fig. 7c) indicated variability or disturbance of the U-Pb system in these crystals and asked for a more detailed and systematic investigation. Precise U-Pb dating was carried out on a transect through the 1.5 cm long crystal ZFG2b: a slice of some 500 μm width and 200 μm thickness was cut from the crystal already embedded in epoxy resin (see Fig. 3) and manu-

ally fragmented producing fragments numbered 1 to 10 (inset Fig. 7d). Each of these fragments representing several hundred to 1000 μg of zircon material was further fragmented with tweezers to arrive at sample sizes of a few micrograms suitable for ID-TIMS analysis. Several sub-fragments were randomly selected from six of the fragments, chemically abraded and analyzed. The $^{206}\text{Pb}/^{238}\text{U}$ dates scatter over 4.5 Ma, between 200.7 ± 0.24 and 205.1 ± 0.22 Ma (2σ). The oldest dates were found in the central portions 5 and 6, the youngest in the marginal fragments 1, 8, and 9. For comparison, the two youngest LA-ICP-MS spot dates were obtained from the oscillatory rim of fragment 1.

ZFG3. Twelve zircon crystals have been analyzed, forming two sub-populations according to their U concentration: pink zircon contains 400–570 ppm U, whereas colorless zircon shows higher concentrations between 730 and 1200 ppm. $^{206}\text{Pb}/^{238}\text{U}$ ages scatter between 189.0 ± 0.14 and 189.9 ± 0.15 Ma (2σ), without systematic distribution between the two zircon types. No mean age can therefore be calculated from these data and the scatter needs to be explained by natural processes.

Initial Hf isotope composition of zircon

Some of the trace element fractions from the U-Pb anion exchange column chemistry were analyzed for initial Hf isotopic composition. One fragment of ZFG1 has an ϵHf of 8.9 ± 0.1 (all uncertainties at 2σ); analysis of five fragments of crystal ZFG2a resulted in ϵHf of 8.9 ± 0.7 to 9.8 ± 0.4 (Supplemental Table 3¹). The fragments of the U-Pb dating transect through crystal ZFG2b were also analyzed for Hf isotope composition (Supplemental Table 3¹). A total of 24 analyses from 6 fragments have been carried out in one measurement sequence starting with fragment 1.1 and ending with 9.3, showing a systematic scatter with higher ϵHf of 7.4–8.0 along the rims, and a low- ϵHf zone at values of 7.0 in fragment 6 (± 0.2 – 0.3 typical uncertainties at 2σ ; Fig. 8).

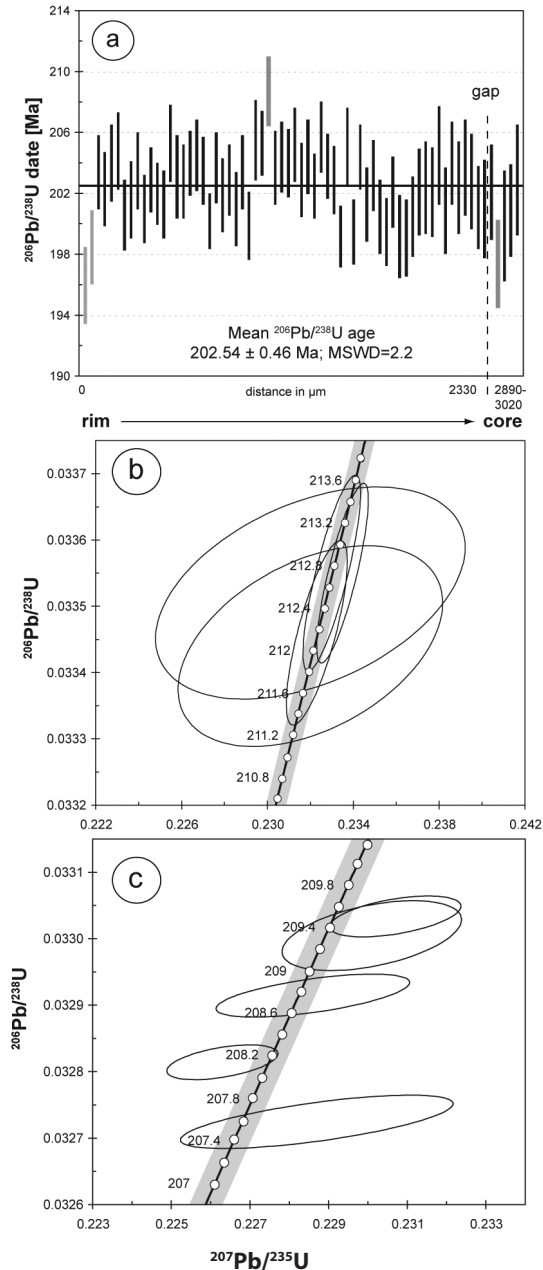


FIGURE 7. Results of U-Pb age determinations: (a) $^{206}\text{Pb}/^{238}\text{U}$ age ranked plot with results from laser ablation ICP-MS spot analyses along a core-rim profile through zircon ZFG2b; data are shown with 2σ uncertainty bars, analyses marked in gray are excluded from mean age calculations; (b) concordia diagram with results of CA-ID-TIMS analyses from crystal ZFG1; (c) concordia diagram with results of CA-ID-TIMS analyses from crystal ZFG2a; (d) concordia diagram with CA-ID-TIMS results from a transect through ZFG2b, shown as inset. The color coding and numbering of the error ellipses refers to the fragment colors and numbers shown in the inset. The transect is indicated in Figure 3; (e) concordia diagram with results of CA-ID-TIMS analyses of zircons from sample ZFG3.

enriched compared to depleted mantle at 200 Ma. The six pink zircon crystals from sample ZFG3 have significantly lower ϵ_{Hf} at $6.4\text{--}6.7 \pm 0.3$ (Supplemental Table 3¹).

Oxygen isotope analysis

Oxygen isotopic compositions have been determined on 0.5 to 1 mg of zircon material from crystals ZFG2a and ZFG2b, using laser fluorination stable isotope mass spectrometry (Supplemental Table 4¹). Four random fractions of ZFG2a have $\delta^{18}\text{O}$ (VSMOW) values of 6.05–6.14‰ (all values $\pm 0.1\%$ at 2σ); the transect through crystal ZFG2b yielded a non-systematic across-grain variation of $\delta^{18}\text{O}$ between 5.98 and 6.25‰. All determined values are distinctly higher than a value of $5.3 \pm 0.3\%$ typical for zircon in equilibrium with a melt from a depleted mantle source, and for example, reported from kimberlite zircon megacrysts (Valley et al. 1998). The $\delta^{18}\text{O}$ values show no systematic core-

The scatter is significant; to test for a possible instrumental drift and to quantify internal reproducibility, sub-fragment 5.4 has been analyzed in duplicate at the very end of this measurement series, indicated by asterisks in Figure 8, and a total of 21 JMC-475 standard solutions have been measured before, in between and after the unknowns. The deviation between the duplicates and the standard results indicate that a potential instrumental drift would be within analytical uncertainty of any individual analysis and would not influence the zone of low ϵ_{Hf} values in the center. The observed systematics is in line with a weak zonation indicated by trace elements (Fig. 6a). The Hf isotopic composition of the zircons points to a source that is slightly

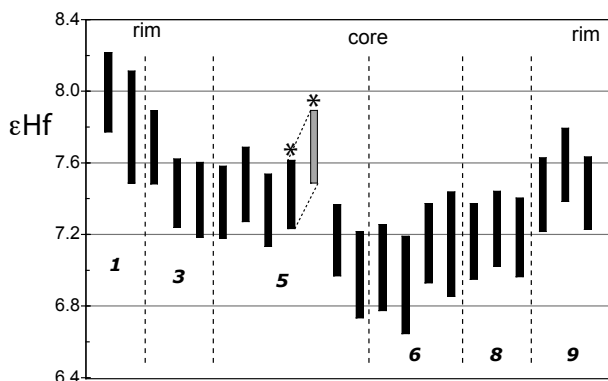


FIGURE 8. Hf isotope analyses from fragments of crystal ZFG2b. The two analyses marked by an asterisk indicate a duplicate analysis (gray bar), the duplicate being analyzed at the very end of this series. Despite some possible instrumental drift, a central zone consisting of fragments 5 and 6 with clearly lower ϵHf can be identified.

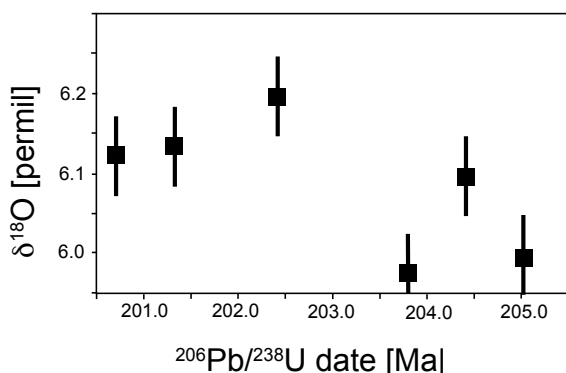


FIGURE 9. Variation of $\delta^{18}\text{O}$ values with $^{206}\text{Pb}/^{238}\text{U}$ date of transect through ZFG2b shown in Figure 7d, inset. Uncertainty is 1 St.dev. of 4 NBS-28 quartz analyses.

rim correlation; for fragments of ZFG2b a $^{206}\text{Pb}/^{238}\text{U}$ date was obtained, the oxygen isotope data may indicate a weak tendency of higher $\delta^{18}\text{O}$ values toward lower ages (Fig. 9).

DISCUSSION

Formation of the nepheline pegmatites

Nepheline-bearing pegmatites are usually associated to large masses of nepheline-syenite intrusions that were differentiated from mantle-derived parental melts (e.g., Andersen et al. 2010). Formation by direct melting of a metasomatized mantle is unlikely, because of their negligible Mg contents and very high degrees of enrichments in elements such as K, Na, U, Th, and Zr. In addition, there are no mantle-derived enclaves or xenocrysts in the studied rock samples. We may envisage a multi-stage evolution of (1) partial melting of a metasomatic, CO_2 -enriched, amphibole-bearing and/or carbonated lithospheric mantle source to form an olivine nephelinitic or basanitic precursor magma (Francis and Ludden 1990, 1995; Price et al. 2003; Jung et al. 2006; Ulianov et al. 2007), (2) formation of K, U, Th-enriched nepheline-syenitic magmas through fractional crystallization of

olivine and clinopyroxene from the basanitic precursor, followed by (3) exsolution of a volatile and LILE/HFSE-rich residual magma forming the pegmatites. This exsolution of volatiles in nepheline syenite system was previously described as being responsible for violent “mantle explosions,” fracturing overlying rocks and driving volatile and residual liquid- and incompatible element enriched magma upward into previously crystallized magmas or into host rocks, as inferred for the formation of incompatible element-rich peralkaline rocks in the Ilímaussaq alkaline complex (Sørensen et al. 2011).

The studied pegmatite bodies of Finero have typical alkaline geochemical characteristics with elevated Na, K, Zr, and P contents, and high Zr/Hf ratios in zircon; their mineralogy, particularly the abundance of biotite and the presence of corundum and zircon is characteristic of miaskitic pegmatites. The absence of any resorption textures indicates that the parental magmas remained saturated with respect to zircon and the melts, therefore did not evolve toward apatitic compositions (Andersen et al. 2010). Initial ϵHf values of +9 to +6.5 point to a metasomatically enriched mantle as a source of the melts, in line with ϵNd and $^{87}\text{Sr}/^{86}\text{Sr}$ values of +5.4 and 0.7042, respectively, reported by Stähle et al. (1990) from a syenite pegmatite from Rio Creves near the southwestern termination of the complex (Fig. 1).

Our new and published U-Pb age determinations suggest that smallest volumes of highly evolved melts emplaced as alkaline pegmatites over 22.5 Ma (212.5 to 189 Ma) in the area around the Finero complex. The large age variation found within the same zircon grains of pegmatite ZFG2 may be interpreted as protracted or repeated growth periods, which is difficult to reconcile with the maximum 100 m³ size of the pegmatites, unless the pegmatite vein acted as a melt/fluid channelway for a long period of time. Alternatively or additionally, open-system behavior of the U-Pb system in zircon at high temperature of the lower crust has to be considered to explain this data. We first evaluate whether the planar fractures encountered in zircons of ZFG1 and ZFG2 may have facilitated lead loss at high temperatures.

Origin of the planar fractures in zircon

Planar fractures (PFs) in zircon and other minerals have been extensively documented and discussed in the literature from various impact sites (e.g., French 1998; Kamo et al. 1996; Cavosie et al. 2010) and were experimentally produced above shock pressures of 20 GPa (Wittmann et al. 2009). The reported PF values in our pegmatite zircons are similar to those described by Cavosie et al. (2010; their Fig. 6) from shocked zircon of the Vredefort dome, but at considerably greater spacing. Planar fractures in terrestrial zircon have been known from zircon (mega)crystals in kimberlites. According to Kresten et al. (1975), kimberlitic zircons show “one or several directions of perfect cleavage, in contrast to the zircons from most other sources.” These authors also emphasize the absence of a crystallographic control on the orientation of the “cleavages” and suggest that it is appropriate to describe them as a parting. Stress at mantle depths has been invoked as a possible explanation for these findings. Dawson (1980) considers parting as a feature characteristic of kimberlitic zircons in general. Later, Schärer et al. (1997) reinforced and interpreted planar and mosaic textures from kimberlitic mega-

zircons as a “stress produced feature affecting the megacrysts at great depth.” However, they also suggested that they “may be indicative of very fast decompression in the ascending kimberlite,” this process apparently having no direct relation to the stress conditions of the upper mantle. Planar fractures have never been reported from granulite-facies zircons of the Ivrea Zone or other granulite terrains. Long residence at lower crustal conditions is therefore an unlikely mechanism to form planar fractures.

A tentative explanation, partly consistent with the decompression hypothesis above, invokes volatile saturation at deep crustal or mantle levels. Alkaline magmas are some of the most volatile-enriched magmas, and consequently some of the most explosive magmas known. It is the explosive nature of kimberlite melts, combined with their low density and viscosity, that allows these melts to rise rapidly through the 200 km thick lithosphere, fragment the rocks adjacent to the magma conduit, and form tuffitic breccias inside the pipe. Explosions in phonolite (Price et al. 2003) and nepheline syenite (Sørensen et al. 2011) systems are also well documented. Explosions probably take place during the MARID crystallization as well, irrespective of whether the MARIDs form from lamproitic (Waters 1987) or kimberlitic (Dawson and Smith 1977; Konzett et al. 1998) precursor melts. We therefore propose that these specific “mantle pegmatites” arrived at volatile saturation during the crystallization history.

An “explosion” at mantle or possibly lower crustal pressure conditions may be defined as a sudden pressure release (decompression) at a rate much faster compared to a constant magma ascent. We imagine that this is caused by fracturing and faulting of the surrounding environment, followed by sudden volume increase and forceful injection of the volatile-saturated and LILE, LREE, and HFSE-enriched residual melts into overlying fracture systems. Such processes may send forceful shock waves through their surroundings; the planar fractures in zircon of the two older nepheline syenite pegmatites of Finero (ZFG1 and ZFG2), as well as the above described brecciation of nepheline megacrysts in ZFG2 is consistent with this interpretation. The euhedral shape of all zircons in pegmatites ZFG2 and ZFG3 argues for growth from a zircon saturated liquid as no resorption textures have been observed in CL images. This is in line with the phase with the SiO₂-undersaturated portion of a H₂O-saturated system NaAlSiO₄-KAlSiO₄-SiO₂ (nepheline-kalsilite-quartz) at pressures of ~1.0 GPa, which suggest the presence of a large proportion of melt at 900 °C (Zeng and MacKenzie 1984, 1987; Gupta et al. 2010).

Age record from the pegmatites: Multi-episodic growth vs. lead loss by volume diffusion

The U-Pb data presented here are to some extent in contradiction to the present understanding of the U-Pb isotopic system in zircon, and needs to be discussed in the light of U-Pb system behavior at elevated temperatures and pressures. Both LA-ICP-MS and CA-ID-TIMS U-Pb data on the two crystals (ZFG2a and ZFG2b) indicate within-grain age variation of several millions of years. LA-ICP-MS U-Pb dating only is capable of distinguishing between a ca. 197 Ma old, 200 μm wide oscillatory-zoned rim (Fig. 4d), and the rest of the grain with an average age of 202.54 ± 0.46 Ma (Fig. 7a). The 4.5 Ma U-Pb age scatter obtained by CA-ID-TIMS may therefore be explained by mixing of growth

zones within one analyzed fragment. Below, we discuss the question whether this age variation in the studied zircon grains is caused by (1) protracted, continuous, or episodic growth; or (2) by post-crystallization loss of radiogenic lead due to volume and fast pathway diffusion:

An argument for protracted growth is the fact that three growth generations can be distinguished from trace element concentrations, Hf isotopes, and CL images:

(1) A Th-U-REE depleted zone with higher CL intensity, low Th/U ratios, and low εHf values that forms the cores (Figs. 6a, 6b, and 8)

(2) A Th-U-REE enriched zone with low luminescence and slightly higher εHf values, forming the intermediate rims (Figs. 6a, 6b, and 8). The divide between growth generations 1 and 2 seems to be sharp.

(3) Outermost oscillatory-zoned ~200 μm wide rim with overall slightly lower REE concentrations (Figs. 4d and 5c), which obviously crystallized several million years later (Fig. 7a).

These observations are in agreement with an interpretation invoking growth zoning. Oxygen isotope values, however, record a narrow range of values between 5.98 and 6.25‰, without any systematic core-rim variation nor a discernible covariation with U-Pb date (Supplemental Table 4¹; Fig. 9). The narrow range of δ¹⁸O values may be explained by slight variation of oxygen isotope composition of the melts, from which the zircon crystallized, but it is close to the analytical precision of the method used and we favor homogeneous oxygen isotope distribution across the grain. Complete post-crystallization ¹⁸O/¹⁶O isotope homogenization at $P_{H_2O} = 10$ kb and 900 °C is possible (Cherniak and Watson 2003), if we assume spacing of a few hundred micrometers of the planar fractures as fast-diffusion pathways.

Another important issue is whether the large size of these zircons implies very long crystallization periods, which could be reflected by the spread in U-Pb ages. Radial crystallization rates of zircon range between 10⁻¹³ cm/s (measured value from a volcanic rock; Schmitt et al. 2011) to 10⁻¹⁷ cm/s (inferred minimum value from a kinetic model; Watson 1996). For uninterrupted, continuous growth of an equant-shaped zircon of 1 cm diameter these values translate into growth durations between 530 Ka and 1.6 Ga. Assuming that an analytically determined date is more accurate than kinetic model calculations (i.e., adopting the values from Schmitt et al. 2011), we argue that the growth of the ZFG zircons was considerably shorter than the age span determined by our high precision U-Pb data. In addition, growing a zircon crystal continuously over a period of some 4.5 Ma would in fact imply that high temperatures at zircon saturation were maintained throughout this period. This seems improbable for melt volumes that obviously did not exceed a few tens to hundreds of cubic meters.

We further evaluate the hypothesis that the above described U-Pb age dispersion of some 4.5 Ma reported by ID-TIMS from crystal ZFG2b may be due to continuous loss of radiogenic Pb through volume diffusion at elevated temperatures: This loss is unrelated to any decay damage effect, and instead reflects a steady state process occurring at elevated temperatures at mantle or lower crustal depths. To test this hypothesis, we modeled volume diffusion through zircon using the equations of Crank (1975) and the diffusion parameters of Cherniak and Watson

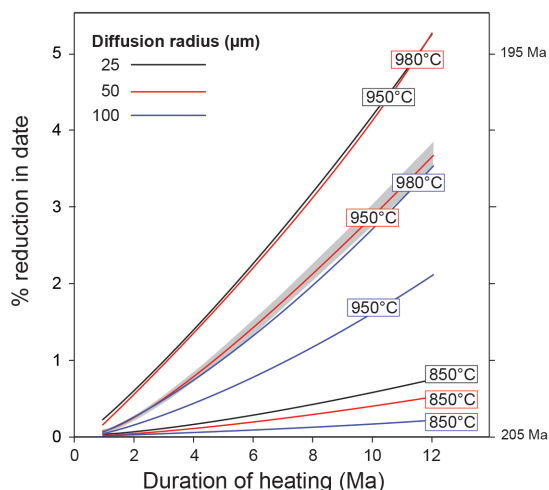


FIGURE 10. Diffusion model calculations based on the diffusion parameters of Cherniak and Watson (2001) and the equations from Crank (1975); for discussion of the parameters, see text.

(2001; see details in the electronic supplementary materials¹), assuming a spherical morphology. We constrained the temperatures in our model to between 850 and 980 °C, a very sensitive temperature range with respect to volume diffusion of Pb in zircon. These values are close to sapphirine-spinel equilibrium temperatures of reported igneous sapphirine within ca. 200 Ma old leucogabbro dikes within the phlogopite peridotite (Sills et al. 1983, Giovanardi et al. 2013; Grieco et al. 2001).

As a minimal diffusion domain size we may adopt 100 μm (i.e., 50 μm diffusion radius), and we also show computed curves for 25 and 100 μm radii (Fig. 10). The results demonstrate that we need a residence of some 9.5 Ma at temperatures of 950 °C, assuming a 50 μm diffusion radius, to reproduce the 4.5 Ma age scatter found in ZFG2b by ID-TIMS U-Pb dating (Fig. 7d). Reducing the temperatures to 900 or 850 °C, would only produce some 3 and 0.4 Ma age reduction, respectively (Fig. 10). The EBSD misorientation map of grain ZFG2c (Fig. 5) did not reveal any mosaic texture with subgrains below 100 μm size, which does not give support to adopt shorter diffusion distances for our model calculations. We feel that the adopted temperatures are unrealistically high to be representative for a regional metamorphic temperature in the lower crust between 205 and 195 Ma; the occurrence of igneous sapphirine in a few centimeters thick leucogabbro dikes would only cause transient temperature peaks of shortest duration (Giovanardi et al. 2013).

This diffusion-induced age dispersion is equally insufficient to explain the 0.8 Ma scatter of 500–1000 μm sized, single zircon crystals in sample ZFG3, which interestingly do not show any planar fracturing and show sector zoning typical for undisturbed growth at high temperatures and pressures (Figs. 4g and 4h). The five ID-TIMS analyses of zircon ZFG1 do not reveal any age scatter (Fig. 7b) despite the abundance of planar fractures visible in Figure 2a. It may be argued that the elevated uncertainties of the 1999 analytical procedures applied to ZFG1 are masking minor scatter in the ²⁰⁶Pb/²³⁸U data from this sample.

In conclusion, we consider partial loss of radiogenic Pb by

volume-diffusion as being of marginal importance for explaining the observed age scatter through crystals ZFG2b and zircons from sample ZFG3. These age differences have, therefore, to be considered to be caused by protracted crystal growth.

IMPLICATIONS

Unique megacrystic zircon from alkaline, nepheline-bearing, miaskitic pegmatites from the Finero complex situated at the eastern termination of the Ivrea Zone are described and their geochemical compositions interpreted. These pegmatites represent smallest volumes of highly fractionated partial melts from a metasomatized mantle that intruded the lower crust of the Adriatic plate in the late Triassic to early Jurassic between 212.5 and 190 Ma in at least three pulses. This occurrence is to our knowledge the first high-pressure miaskitic pegmatite reported. Phenomena of hydrodynamic fracturing in one of the pegmatites suggest that the LILE and HFSE enriched and volatile-saturated residual melts became strongly overpressured, underwent boiling, and explosive volatile release. Zircons of this pegmatite show several orientations of planar fractures that are partly filled by albite and zircon. We therefore provide here an example for the occurrence of terrestrial non-impact related planar fractures in zircon, tentatively interpreted as the result of the explosive volatile release, and subsequent crystallization of albite and zircon from vapor-saturated melt.

The described zircons do not have simple crystallization ages, but show up to million-year large age dispersions in one single crystal. Model calculations of continuous loss of radiogenic lead under lower-crustal conditions at elevated temperature may only explain a minor component of the observed scatter of U-Pb ages along the concordia. Unrealistically high regional temperatures of 950 °C during 9.5 Ma are needed to reproduce the 4.5 Ma reduction in age, based on a 100 μm spacing of planar fractures acting as fast diffusion pathways. We therefore conclude that the planar fractures do not play a significant role in removal of radiogenic Pb and that the observed age dispersions are reflecting continuous or episodic growth of zircon, in agreement with weak core to rim zoning in U, Th, P, and REE concentrations, and the systematic variations in Nb/Ta and Th/U ratios, CL intensity and O,Hf isotope compositions.

Intrusion of miaskite melts over more than 20 Ma in Triassic times marks a protracted period of heat advection into the lower crust of the Ivrea Zone. This may explain widespread disturbance of isotope systems in minerals, which closed after the Permian granulite-facies metamorphism and subsequent lower-crustal, mafic magmatism.

ACKNOWLEDGMENTS

The authors thank M. Senn and M. Chiaradia (Geneva) for technical support. R. Spikings is acknowledged for contributing the diffusion calculations, A. Gerdes (Frankfurt) for hosting U.S. at JWU University for Hf isotopic analyses. The Swiss National Science Foundation is acknowledged for funding the research carried out at the universities of Geneva and Lausanne. The manuscript benefitted from very helpful comments of the two journal reviewers B. Schoene and A. Zanetti.

REFERENCES CITED

- Andersen, T., Erambert, M., Larsen, A.O., and Selbekk, R.S. (2010) Petrology of nepheline syenite pegmatites in the Oslo Rift, Norway: Zirconium silicate mineral assemblages as indicators of alkalinity and volatile fugacity in mildly aegpaitic magma. *Journal of Petrology*, 51, 2303–2325.
- Arzamastsev, A., Yakovenchuk, V., Pakhomovsky, Y., and Ivanyuk, G. (2008) The

- Khibina and Lovozero alkaline massifs: Geology and unique mineralization. 33rd International Geological Congress Excursion No. 47, Geological Institute of the Russian Academy of Science, Apatity, Russia. 58 p.
- Ashwal, L.D., Armstrong, R.A., Roberts, R.J., Schmitz, M.D., Corfu, F., Hetherington, C.J., Burke, K., and Gerber, M. (2007) Geochronology of large zircons from nepheline-bearing gneisses as constraints on tectonic setting: an example from southern Malawi. *Contributions to Mineralogy and Petrology*, 153, 389–403.
- Bayly, B., Reid, A., and Gurney, J.J. (1979) Zircon-bearing rocks from the Kimberley mines. Abstracts of the 18th Congress of the Geological Society of South Africa, 19–23.
- Besairie, H. (1966) Les Gîtes Minéraux de Madagascar. *Annales Géologiques de Madagascar*, XXXIV, Tananarive, 822 p.
- Black, L.P., and Gulson, B.L. (1978) The age of the Mud Tank carbonatite, Strangways Range, Northern Territory. *BMR Journal of Australian Geology and Geophysics*, 3, 227–232.
- Cavosie, A.J., Quintero, R.R., Radovan, H.A., and Moser, D.E. (2010) A record of ancient cataclysm in modern sand: Shock microstructures in detrital minerals from the Vaal River, Vredefort Dome, South Africa. *Geological Society of America Bulletin*, 122, 1968–1980.
- Cherniak, D., and Watson, E. (2001) Pb diffusion in zircon. *Chemical Geology*, 172(1), 5–24.
- (2003) Diffusion in zircon. *Reviews in Mineralogy and Geochemistry*, 53(1), 113–143.
- Cherniak, D.J., Manchester, J., and Watson, E.B. (2007) Zr and Hf diffusion in rutile. *Earth and Planetary Science Letters*, 261(1–2), 267–279.
- Corfu, F., Hanchar, J., Hoskin, P., and Kinny, P. (2003) Atlas of Zircon Textures. *Reviews in Mineralogy and Geochemistry*, 53, 469–500.
- Crank, J. (1975) *The Mathematics of Diffusion*, 414 p. Clarendon Press, Oxford.
- Crohn, P.W., and Moore, D.H. (1984) The Mud Tank carbonatite, Strangways Range, central Australia. *BMR Journal of Australian Geology and Geophysics*, 9, 13–18.
- Dawson, J.B. (1980) *Kimberlites and their Xenoliths*. Springer Verlag, Berlin, 272 p.
- Dawson, J.B., and Smith, J.V. (1977) The MARID (mica-amphibole-rutile-ilmenite-diopside) suite of xenoliths in kimberlite. *Geochimica et Cosmochimica Acta*, 41, 309–323.
- Francis, D., and Ludden, J. (1990) The mantle source for olivine nephelinite, basanite, and alkaline olivine basalt at Fort Selkirk, Yukon, Canada. *Journal of Petrology*, 31, 371–400.
- (1995) The signature of amphibole in mafic alkaline lavas, a study in the Northern Canadian Cordillera. *Journal of Petrology*, 36, 1171–1191.
- French, B.M. (1998) *Traces of a Catastrophe: A Handbook of Shock-Metamorphic Effects in Terrestrial Meteorite Impact Structures*. LPI Contribution No. 954, Lunar and Planetary Institute, Houston, 120 p.
- Gebauer, D., Schmid, R., von Quadt, A., and Ulmer, P. Oligocene, (1992) Permian and Panafrican zircon ages from rocks of the Balmuccia Peridotite and of the Lower Layered Group in the Ivrea Zone. *Schweizerische Mineralogische und Petrographische Mitteilungen*, 72, 113–122.
- Giovanardi, T., Morishita, T., Zanetti, A., Mazzucchelli, M., and Vannucchi, R. (2013) Igneous sapphirine as a product of melt-peridotite interactions in the Finero phlogopite-peridotite massif, Western Italian Alps. *European Journal of Mineralogy*, 25, 17–31.
- Girlanda, F., Antognini, M., Weiss, S., and Praeger, M. (2007) Zirkon aus Nephelin-Pegmatiten im Peridotit Finero-Centovalli (Schweiz). *Lapis*, 32/6, 13–23.
- Grieco, G., Ferrario, A., von Quadt, A., Koepfel, V., and Mathez, E.A. (2001) The zircon-bearing chromitites of the phlogopite peridotite of Finero (Ivrea Zone, Southern Alps): Evidence and geochronology of a metasomatized mantle slab. *Journal of Petrology*, 42, 89–101.
- Grimes, C.B., John, B.E., Cheadle, M.J., Mazdab, F.K., Wooden, J.L., Swapp, S., and Schwartz, J.J. (2009) On the occurrence, trace element geochemistry, and crystallization history of zircon from in situ ocean lithosphere. *Contributions to Mineralogy and Petrology*, 158, 757–783.
- Gupta, A.K., Dwivedi, M.M., Bhattachariya, H., and Dasgupta, S. (2010) Silica-undersaturated portion of the system nepheline – kalsilite – SiO₂ at 2 GPa [P(H₂O) = P(Total)]. *Canadian Mineralogist*, 48, 1297–1313.
- Hartmann, G., and Wedepohl, K.H. (1993) The composition of peridotite tectonites from the Ivrea Complex, northern Italy—residues from melt extraction. *Geochimica et Cosmochimica Acta*, 57, 1761–1782.
- Hollis, J.D., and Sutherland, F.L. (1985) Occurrences and origins of gem zircons in eastern Australia. *Records of the Australian Museum*, 36, 299–311.
- Hunziker, J.C. (1974) Rb-Sr and K-Ar age determination and the alpine tectonic history of the Western Alps. *Memorie degli Istituti di Geologia e Mineralogia dell' Università di Padova*, 31, 5–55.
- Jung, C., Jung, S., Hoffer, E., and Berndt, J. (2006) Petrogenesis of tertiary mafic alkaline magmas in the Hoheifel, Germany. *Journal of Petrology*, 47, 1637–1671.
- Kamo, S.L., Reimold, W.U., Krogh, T.E., and Colliston, W.P. (1996) A 2.023 Ga age for the Vredefort impact event and a first report of shock metamorphosed zircons in pseudotachylitic breccias and granophyre. *Earth and Planetary Science Letters*, 144, 369–387.
- Konerup-Madsen, J., and Rose-Hansen, J. (1984) Composition and significance of fluid inclusions in the Ilmaussaq peralkaline granite, south Greenland. *Bulletin de Minéralogie*, 107, 317–326.
- Konzett, J., Armstrong, R.A., Sweeney, R.J., and Compston, W. (1998) The timing of MARID metasomatism in the Kaapvaal mantle: an ion probe study of zircons from MARID xenoliths. *Earth and Planetary Science Letters*, 160, 133–145.
- Kresten, P., Fels, P., and Berggren, G. (1975) Kimberlitic zircons—a possible aid in prospecting for kimberlites. *Mineralium Deposita*, 10, 47–56.
- Lacroix, A. (1922) *Mineralogie de Madagascar, Tome I. Géologie-Minéralogie descriptive*. Paris, 624 p.
- Linnen, R.L., and Keppler, H. (2002) Melt composition control of Zr/Hf fractionation in magmatic processes. *Geochimica et Cosmochimica Acta*, 66, 3293–3301.
- Lu, M., Hofmann, A.W., Mazzucchelli, M., and Rivalenti, G. (1997) The mafic-ultramafic complex near Finero (Ivrea-Verbano Zone), II. Geochronology and isotope geochemistry. *Chemical Geology*, 140, 223–235.
- Markl, G., Marks, M., Schwinn, G., and Sommer, H. (2001) Phase equilibrium constraints on intensive crystallization parameters of the Ilmaussaq complex, South Greenland. *Journal of Petrology*, 42, 2231–2257.
- Mayer, A., Mezger, K., and Sinigoi, S. (2000) New Sm–Nd ages for the Ivrea-Verbano Zone, Sesia and Sessera valleys (Northern-Italy). *Journal of Geodynamics*, 30, 147–166.
- Page, F.Z., Fu, B., Kita, N.T., Fournelle, J., Spicuzza, M.J., Schulze, D.J., Viljoen, F., Basei, M.A.S., and Valley, J.W. (2007) Zircon from kimberlite: New insights from oxygen isotopes, trace elements, and Ti in zircon thermometry. *Geochimica et Cosmochimica Acta*, 71, 3887–3903.
- Pedersen, R.B., Dunning, G.R., and Robins, B. (1989) U-Pb ages of nepheline syenite pegmatites from the Seiland Magmatic Province, N Norway. In R.A. Gayer, Ed., *The Caledonide Geology of Scandinavia*, p. 3–8. Graham and Trotman, London.
- Peressini, G., Quick, J., Sinigoi, S., Hofmann, A., and Fanning, M. (2007) Duration of a large mafic intrusion and heat transfer in the lower crust: a SHRIMP U-Pb zircon study in the Ivrea-Verbano Zone (Western Alps, Italy). *Journal of Petrology*, 48, 1185–1218.
- Popov, V.A., and Popova, V.I. (2006) *Ilmeny: Mineralogy of Pegmatites*. *Mineralogical Almanac*, 9. Ocean Pictures, Littleton, Colorado. 156 p.
- Price, R.C., Cooper, A.F., Woodhead, J.D., and Cartwright, I. (2003) Phonolitic diatremes within the Dunedin Volcano, South Island, New Zealand. *Journal of Petrology*, 44, 2053–2080.
- Rutter, E., Brodie, K., James, T., and Burlini, L. (2007) Large-scale folding in the upper part of the Ivrea-Verbano zone, NW Italy. *Journal of Structural Geology*, 29, 1–17.
- Schaltegger, U., Fanning, C., Günther, D., Maurin, J., Schulmann, K., and Gebauer, D. (1999) Growth, annealing and recrystallization of zircon and preservation of monazite in high-grade metamorphism: conventional and in-situ U-Pb isotope, cathodoluminescence and microchemical evidence. *Contributions to Mineralogy and Petrology*, 134, 186–201.
- Schärer, U., Corfu, D., and Demaiffe, D. (1997) U-Pb and Lu-Hf isotopes in baddeleyite and zircon megacrysts from the Mbuji-Mayi kimberlite: constraints on the subcontinental mantle. *Chemical Geology*, 143, 1–16.
- Schmitt, A.K., Danišik, M., Evans, N.J., Siebel, W., Kiemle, E., Aydin, F., and Harvey, J.C. (2011) Acigöl rhyolite field, Central Anatolia (part 1): high-resolution dating of eruption episodes and zircon growth rates. *Contributions to Mineralogy and Petrology*, 162, 1215–1231.
- Siena, F., and Coltorti, M. (1989) The petrogenesis of a hydrated mafic—ultramafic complex and the role of amphibole fractionation at Finero (Italian Western Alps). *Neues Jahrbuch für Mineralogie, Monatshefte*, 6, 255–274.
- Sills, J.D., Ackermann, D., Herd, R.K., and Windley, B.F. (1983) Bulk composition and mineral parageneses of sapphirine-bearing rocks along a gabbro-lherzolite contact at Finero, Ivrea Zone, N Italy. *Journal of Metamorphic Geology*, 1, 337–351.
- Sørensen, H., Bailey, J.C., and Rose-Hansen, J. (2011) The emplacement and crystallization of the U–Th–REE-rich apatitic and hyperapatic lujuvrites at Kvanebjerg, Ilmaussaq alkaline complex, South Greenland. *Bulletin of the Geological Society of Denmark*, 59, 69–92.
- Stähle, V., Frenzel, G., Kober, B., Michard, A., Puchelt, H., and Schneider, W. (1990) Zircon syenite pegmatites in the Finero peridotite (Ivrea zone): evidence for a syenite from a mantle source. *Earth and Planetary Science Letters*, 101, 196–205.
- Ulianov, A., Muntener, O., Ulmer, P., and Pettke, T. (2007) Entrained macrocryst minerals as a key to the source region of olivine nephelinites: Humberg, Kaiserstuhl, Germany. *Journal of Petrology*, 48, 1079–1118.
- Upton, B.G.J., and Emeleus, C.H. (1987) *Mid-Proterozoic alkaline magmatism in southern Greenland: the Gardar province*. Geological Society, London, Special Publications, 30, 449–471.
- Valley, J.W., Kinny, P.D., Schulze, D.J., and Spicuzza, M.J. (1998) Zircon megacrysts from kimberlite: oxygen isotope variability among mantle melts. *Contributions to Mineralogy and Petrology*, 133, 1–11.

- von Quadt, A., Ferrario, A., Diella, V., Hansmann, G., Vavra, G., and Köppel, V. (1993) U-Pb ages of zircons from chromitites of the phlogopite peridotite of Finero, Ivrea zone, N-Italy. *Schweizerische Mineralogische und Petrographische Mitteilungen*, 73, 137–138.
- Wang, X., Griffin, W., and Chen, J. (2010) Hf contents and Zr/Hf ratios in granitic zircons. *Geochemical Journal*, 44, 65.
- Waters, F.G. (1987) A suggested origin of MARID xenoliths in kimberlites by high-pressure crystallization of an ultrapotassic rock such as lamproite. *Contributions to Mineralogy and Petrology*, 95, 523–533.
- Watson, E.B. (1996) Dissolution, growth and survival of zircons during crustal fusion: Kinetic principles, geological models and implications for isotopic inheritance. *Geological Society of America Special paper*, 315, 43–56.
- Weiss, S. (2011) Seiland, Norwegen—eine legendäre Zirkonfundstelle am Alta-Fjord, Finnmark. *Lapis*, 36/11, 15–19.
- Weiss, S., Fehr, T., Ansermet, S., and Meisser, N. (2007) Zirkonführende Nephelinpegmatite im Centovalli, Südschweiz: Struktur, Mineralogie und Kristallisationsabfolge. *Lapis*, 32/6, 24–30.
- Wittmann, A., Schmitt, R.T., Hecht, L., Kring, D.A., Reimold, W.U., and Povenmire, H. (2009) Petrology of impact melt rocks from the Chesapeake Bay crater, USA. In G.S. Gohn, C. Koeberl, K.G. Miller, and W.U. Reimold, Eds., *The ICDP-USGS Deep Drilling Project in the Chesapeake Bay Impact Structure: Results from the Eyreville Core Holes*. Geological Survey of America Special paper, 458, 377–396.
- Yu, Y., Xu, X., and Chen, X. (2010) Genesis of zircon megacrysts in Cenozoic alkali basalts and the heterogeneity of subcontinental lithospheric mantle, eastern China. *Mineralogy and Petrology*, 100, 75–94.
- Zack, T., Stockli, D.F., Luvizotto, G.L., Barth, M.G., Belousova, E., Wolfe, M.R., and Hinton, R.W. (2011) In situ U–Pb rutile dating by LA-ICP-MS: ^{208}Pb correction and prospects for geological applications. *Contributions to Mineralogy and Petrology*, 162, 515–530.
- Zanetti, A., Mazzucchelli, M., Sinigoi, S., Giovanardi, T., Peressini, G., and Fanning, M. (2013) SHRIMP U-Pb zircon Triassic Intrusion Age of the Finero Mafic Complex (Ivrea-Verbano Zone, Western Alps) and its geodynamic implications. *Journal of Petrology*, 54, 2235–2265.
- Zeng, R.S., and MacKenzie, W.S. (1984) Preliminary report on the system $\text{NaAlSi}_3\text{O}_8\text{-KAlSi}_3\text{O}_8\text{-SiO}_2\text{-H}_2\text{O}$ at $P(\text{H}_2\text{O})=5\text{ kbar}$. *Bulletin de Minéralogie*, 107, 571–577.
- (1987) Equilibrium phase diagram of the system $\text{NaAlSi}_3\text{O}_8\text{-KAlSi}_3\text{O}_8\text{-SiO}_2\text{-H}_2\text{O}$ at $P(\text{H}_2\text{O})=5\text{ kbar}$. *Scientia Sinica, Series B*, 30, 198–211.

MANUSCRIPT RECEIVED OCTOBER 15, 2013

MANUSCRIPT ACCEPTED JUNE 7, 2014

MANUSCRIPT HANDLED BY DAVID LONDON